Ultrahigh-pressure form of SiO_2 glass with dense pyrite-type crystalline homology

M. Murakami,[1,2,*] S. Kohara,[3,4,5,6,7,†] N. Kitamura,[8,9] J. Akola,[9,10] H. Inoue,[11] A. Hirata,[12,13,14,15] Y. Hiraoka,[4,15,16,17] Y. Onodera,[4,18] I. Obayashi,[17] J. Kalikka,[9] N. Hirao,[5] T. Musso,[19] A. S. Foster,[19,20] Y. Idemoto,[8] O. Sakata,[3] and Y. Ohishi[5]

[1]*Department of Earth Sciences, ETH Zürich, Zürich 8092, Switzerland*
[2]*Department of Earth and Planetary Materials Science, Tohoku University, Sendai 980-8578, Japan*
[3]*Research Center for Advanced Measurement and Characterization, National Institute for Materials Science (NIMS), Hyogo 679-5148, Japan*
[4]*Center for Materials research by Information Integration (CMI2), Research and Services Division of Materials Data and Integrated System (MaDIS) NIMS, Ibaraki 305-0047, Japan*
[5]*Research and Utilization Division, Japan Synchrotron Radiation Research Institute, Hyogo 679-5198, Japan*
[6]*School of Materials Science, Japan Advanced Institute of Science and Technology, Ishikawa 923-1211, Japan*
[7]*PRESTO, Japan Science and Technology Agency, Tokyo 102-0076, Japan*
[8]*Department of Pure and Applied Chemistry, Faculty of Science and Technology, Tokyo University of Science, Chiba 278-8510, Japan*
[9]*Department of Physics, Tampere University of Technology, FI-33101 Tampere, Finland*
[10]*Department of Physics, Norwegian University of Science and Technology, NO-7481 Trondheim, Norway*
[11]*Institute of Industrial Science, The University of Tokyo, Tokyo 153-8505, Japan*
[12]*Graduate School of Fundamental Science and Engineering, Waseda University, Tokyo 169-8555, Japan*
[13]*Kagami Memorial Research Institute for Materials Science and Technology, Waseda University, Tokyo 169-0051, Japan*
[14]*Mathematics for Advanced Materials-OIL, AIST, Sendai 980-8577, Japan*
[15]*WPI Advanced Institute for Materials Research, Tohoku University, Sendai 980-8577, Japan*
[16]*Kyoto University Institute for Advanced Study, Kyoto University, Kyoto 606-8501, Japan*
[17]*Center for Advanced Intelligence Project, RIKEN, Tokyo 103-0027, Japan*
[18]*Institute for Integrated Radiation and Nuclear Science, Kyoto University, Osaka 590-0494, Japan*
[19]*Department of Applied Physics, Aalto University, FI-00076 Aalto, Finland*
[20]*Division of Electrical Engineering and Computer Science, Graduate School of Natural Science and Technology, Kanazawa University, Kanazawa 920-1192, Japan*

(Received 18 September 2018; revised manuscript received 4 January 2019; published 29 January 2019)

High-pressure synthesis of denser glass has been a longstanding interest in condensed-matter physics and materials science because of its potentially broad industrial application. Nevertheless, understanding its nature under extreme pressures has yet to be clarified due to experimental and theoretical challenges. Here we reveal the formation of OSi_4 tetraclusters associated with that of SiO_7 polyhedra in SiO_2 glass under ultrahigh pressures to 200 gigapascal confirmed both experimentally and theoretically. Persistent homology analyses with molecular dynamics simulations found increased packing fraction of atoms whose topological diagram at ultrahigh pressures is similar to a pyrite-type crystalline phase, although the formation of tetraclusters is prohibited in the crystalline phase. This critical difference would be caused by the potential structural tolerance in the glass for distortion of oxygen clusters. Furthermore, an expanded electronic band gap demonstrates that chemical bonds survive at ultrahigh pressure. This opens up the synthesis of topologically disordered dense oxide glasses.

DOI: 10.1103/PhysRevB.99.045153

I. INTRODUCTION

Silica (SiO_2) has been known as one of the most fundamental and abundant oxides in the Earth, which can usually be yielded as quartz, silica sand, or silica stone in a high-purity condition. Due to this ubiquitous availability and abundant resource around the world, SiO_2 has been extensively utilized as an industrially useful material. SiO_2 glass, with high corrosion resistance, high thermostability, and high optical transparency, is a prototype network-forming glass which can be easily synthesized by various methods and is therefore widely used and a technologically important material. Polyamorphism in SiO_2 glass under pressure is one of the most fascinating and puzzling topics in condensed-matter physics and glass science. Several experimental and theoretical studies have been conducted to clarify the details of polyamorphism [1] in SiO_2 glass under high pressure. However, due to the technical hurdles, the experimental studies have been limited to very low-pressure conditions, which prevents a precise understanding of the pressure effect.

Previous experimental studies on SiO_2 glass have shown anomalous behavior under lower pressures up to ~10 GPa, exhibiting elastic softening [2] and permanent densification [3]. Those densification-related properties are closely related

*Corresponding author: motohiko.murakami@erdw.ethz.ch
†Corresponding author: kohara.shinji@nims.go.jp

to a topological transformation of the tetrahedral network [4] and compaction of a significant amount of interstitial cavities in the SiO_2 glass [5], rather than a change in the coordination number of silicon. At higher pressure, transitions to a much denser state are attributed to changes in short- and intermediate-range ordering associated with the change in oxygen coordination around silicon. Although the details of the coordination state and the pressure conditions under which the coordination changes occur are still a matter of debate [6], it appears that the sixfold-coordinated structure is predominant at 40–45 GPa [7,8] subsequent to a gradual change in the Si-O coordination number from four to six, which begins around 10–20 GPa [8], as inferred by a number of experimental measurements including Raman scattering [9], infrared absorption [10], x-ray diffraction/absorption [7,8,11,12], Brillouin scattering [13,14], x-ray Raman scattering [15], and neutron diffraction measurements [16]. Sato and Funamori [17] have reported that the coordination number of SiO_2 glass remains six at least up to 100 GPa based on the energy-dispersive x-ray diffraction measurements, indicating that SiO_2 glass behaves as the corresponding crystalline phase with sixfold-coordinated structure between 40 and 100 GPa.

Ultrahigh-pressure acoustic wave velocity measurements on SiO_2 glass up to 207 GPa by Brillouin scattering spectroscopic experiment [18] have revealed an anomalous increase in the effect of pressure on acoustic velocity at ∼140 GPa, which was interpreted as a structural transition from a sixfold to higher coordination state of silicon above 140 GPa. A series of computational simulations on SiO_2 glass [19,20] has been conducted subsequently, and they have shown the possible formation of a Si-O coordination state higher than six under ultrahigh-pressure conditions above 100 GPa, which strongly supports the experimental findings [18]. These results suggest that the SiO_2 glass becomes far denser under ultrahigh-pressure conditions than previously envisioned [7,8,17], which significantly reshapes our understanding of the nature of the densification mechanism of SiO_2 glass [1]. However, the change in acoustic wave velocity profile as a function of pressure only indicates a structural anomaly, while it does not provide us with any quantitative structural information. Therefore, it still remains experimentally unresolved whether or not such an anomalous increase in the acoustic velocity at ∼140 GPa corresponds to a structural change associated with the coordination number increase. In addition, it has been believed that the sixfold-coordination state in crystalline SiO_2 retains at least above ∼700 GPa. Clarifying this issue is thus also important to understand the analogy between polymorphism and polyamorphism in silica systems under ultrahigh pressures. Very recently, Prescher *et al.* performed high-pressure x-ray diffraction measurements up to 174 GPa and confirmed that the average coordination number is greater than six at ultrahigh pressures [21], but the atomic structure beyond the first coordination distance and the electronic structure are still unknown.

Here, we report the results of state-of-the-art topological analysis on the basis of atomic configuration obtained by classical molecular dynamics (MD) simulations and density functional theory (DFT) calculations up to 200 GPa. *In situ* synchrotron high-pressure x-ray diffraction measurements support the reliability of simulation. Our supporting analytical methods include the concept of persistent homology [22] and we have placed a special focus on the nature of atomic structure, topology, and electronic structures as a function of pressure. Furthermore, we have put emphasis on a general understanding of pressure-induced modification in the glass structure at the atomistic and electronic level to illustrate a motif for densification in comparison with crystalline phases.

II. EXPERIMENT

A. X-ray diffraction measurements

We performed high-pressure *in situ* x-ray diffraction measurements on the beam line BL10XU at the Japanese synchrotron facility of SPring-8 [23]. Angle-dispersive high-pressure x-ray diffraction spectra were collected on the compressed SiO_2 glass at room temperature in a symmetric diamond anvil cell (DAC) at nine separate runs from 0 to 200 GPa. In each run, a prepressed plate of SiO_2 glass powder was loaded into a 50–100 μm hole, depending on the target pressure condition, drilled in the rhenium gasket without a pressure-transmitting medium. The sample was compressed with 300 μm flat culet and 150 μm beveled culet diamond anvils at the lower five pressures and higher four pressures, respectively. The DAC with a large conical angular aperture used in the present experiments allowed the reliable diffraction patterns to be taken in a large angle up to a maximum 2 of 42°. Pressure was determined using the Raman T_{2g} mode of the diamond anvil [24] or ruby fluorescence pressure scale [25]. An incident x-ray beam was monochromatized, using a diamond double-crystal monochromator, to a beam energy of 49.6 and 49.9 keV. The x-ray beam was collimated to ∼40 μm in diameter and x-ray diffraction spectra of the sample were obtained by an image plate (Rigaku-RAXIS IV^{++}), which has 3000 × 3000 (pixel) dimensions with a pixel size of 100 × 100 μm [23]. Integration of the full-circle scattered x-ray images was performed to give conventional one-dimensional scattered profiles. To subtract the background signals derived mainly from the Compton scattering of the diamond anvils, the background x-ray diffraction pattern was collected for each experimental run after decompression from an empty rhenium gasket hole in a diamond anvil cell after removal of the compressed sample. The Q scale was calibrated using the diffraction pattern from the crystalline CeO_2. The density value of SiO_2 glass under high pressure, which is a key parameter in interpreting measured x-ray diffraction data, was estimated based on the recent results by an x-ray absorption method [7]. The collected data were corrected and normalized to give a Faber-Ziman structure factor using a standard program [26].

B. MD simulation

Molecular dynamics (MD) calculations were performed with a Born-Mayer type of pairwise potentials. The potentials of the term of the Coulomb interactions with the effective charges of Si and O atoms and the repulsive term described by the exponential functions are calculated by the formula

$$\Phi_{ij} = \frac{e^2}{4\pi\varepsilon_0}\frac{Z_i Z_j}{r_{ij}} + B\exp\left(-\frac{r_{ij}}{\rho}\right),$$

where r_{ij} is the interatomic distance between atoms, Z is the effective charge, B is the repulsive parameter, e is the elementary charge, ϵ_0 is the permittivity of vacuum, and ρ is the softness parameter. Table 4 in the Supplemental Material [27] gives the parameters for Z, B, and ρ.

The present calculations were carried out for a system of 3000 (1000 Si + 2000 O) atoms in the unit cell. The volume of the unit cell was determined from the number densities of the SiO_2 glasses under pressures of 10, 31, 46, 83, 109, 140, 170, and 200 GPa. Periodic boundary conditions were used and the long-range Coulomb interaction was treated with Ewald's summation. A time step of 1 fs was used in the Verlet algorithm. The authors of this paper created the program code for the MD simulation.

In the MD simulation, the structural models at different pressures were obtained from random starting atomic configurations. The temperature of the system was kept first at 4000 K for 20 000 time steps, after which the system was cooled down to 293 K during 200 000 time steps. The structural model was finally annealed at 293 K for 20 000 time steps. Five structural models were prepared by repeating the above procedure for the different initial configurations for each condition.

We also tested other classical force fields with the LAMMPS program. The different parameterizations included the ReaxFF [28], COMB [29], CHIK [30] and BKS potentials [31]. None of these worked properly in terms of density and atomic structure under high pressure of 109 GPa. This analysis highlights the intrinsic limitations present in the current interatomic potentials.

C. Topological analysis

1. Cavity analysis

The cavity analysis has been performed as described in the previous literature [32]. The system is divided into a cubic mesh with a grid spacing of 0.10 Å, and the points farther from any atom at a given cutoff (here, 2.1 Å and 2.5 Å) are selected and defined as "cavity domains." Each domain is characterized by a center point where the distance to all neighboring atoms is maximal. The distance cutoff can be varied case by case, and the obtained results (volumes) depend closely on this value.

2. Persistent homology and persistence diagram

Given a set of points in the space, the persistent homology captures its topological multiscale structures, and those identified structures are compactly expressed in the format called persistence diagram. The construction of the persistence diagram follows the process described in Fig. 1(a). We first replace each point with a sphere and increase its radius from zero to sufficiently large value. This process corresponds to the changing resolution of our input data. Then, we record the pair of radii (b, d) at which a void (interstitial, vacancy, cavity) in a specific location appears (birth) and disappears (death), respectively. The persistence diagram is a histogram of the birth-death plane counting of voids at the coordinate (b, d). From this construction, the persistence diagram enables one not only to count the number of voids, but also to characterize those shapes and multiscale

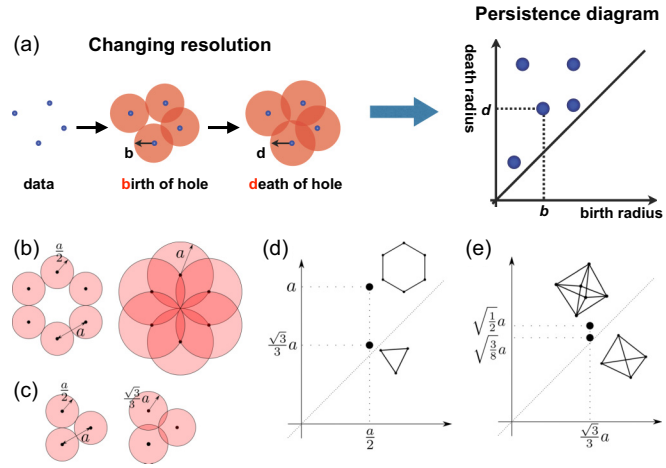

FIG. 1. (a) The increasing sequence of spheres for input data (left). The persistence diagram (right) is obtained as a histogram counting the number of voids on the birth-death plane. (b), (c) The appearance and disappearance of a void for a regular hexagon/triangle. (d) The pairs of birth and death radii for hexagon and triangle in the one-dimensional persistence diagram. (e) The pairs of birth and death radii for tetrahedron and octahedron in the two-dimensional persistence diagram.

properties. To provide the readers with a better understanding of persistence diagrams, we show some examples of birth-death pairs for typical regular structures in Figs. 1(b)–1(e). For regular hexagonal points whose distance between points is a, the void appears at radius $a/2$ and disappears at radius a, as shown in Fig. 1(b). For a regular triangular configuration, the void appears at $a/2$ and disappears at $\sqrt{1/3}a \approx 0.577a$, as shown in Fig. 1(c), and the one-dimensional persistence diagram for regular hexagonal/triangular points is shown in Fig. 1(d). For a two-dimensional persistence diagram, we can similarly evaluate the cavities for a regular tetrahedron and octahedron. The birth and death radii are $\sqrt{1/3}a \approx 0.577a$ and $\sqrt{3/8}a \approx 0.612a$ for a tetrahedron, and $\sqrt{1/3}a \approx 0.577a$ and $\sqrt{1/2}a \approx 0.707a$ for an octahedron, and they are shown in Fig. 1(e). Therefore, the two-dimensional persistence diagram of an fcc crystal with a bond length a displays two sharp peaks at $(0.577a,\ 0.612a)$ and $(0.577a,\ 0.707a)$, corresponding to two types of voids: interstitial tetrahedral and octahedral sites. For further details, we refer the reader to the article on persistent homology [22]. In our work, persistence diagrams are being used for investigating rings and polyhedral formations in atomic configurations. We also note that the detected rings and cavities are recorded during the computation of persistence diagrams, and hence we can explicitly identify their geometric shapes for further analysis.

D. DFT simulations

The CP2K program [33,34] was used to perform the DFT simulations of selected snapshot systems. CP2K employs two representations of the electron density: localized Gaussian and plane-wave (GPW) basis sets. For the Gaussian-based (localized) expansion of the Kohn-Sham orbitals, we use a library of contracted molecularly optimized valence double-zeta plus polarization (m-DZVP) basis sets [35], and the

complementary plane-wave basis set has a cutoff of 550 Rydberg for electron density. The valence electron-ion interaction is based on the norm-conserving and separable Goedecker-Teter-Hutter (GTH) pseudopotentials [36]. The exchange-correlation energy functional employs the generalized gradient corrected approximation of Perdew, Burke, and Ernzerhof (PBE) [37]. The DFT simulations were performed using a simulation box with 3000 atoms where the starting geometry was constructed by the MD simulation mentioned above. The electronic density of states (DOS) and those with projections onto different elements (P-DOS) were calculated after atomic structure relaxation in a fixed volume (pressure). For each element, the effective volumes and charges were estimated from the atomic configuration and the electron density distribution based on the Voronoi method.

III. RESULTS and DISCUSSIONS

A. Structure factors and real-space function

Figure 2(a) shows the x-ray total structure factors $S(Q)$ measured up to 200 GPa, together with the $S(Q)$ derived from the MD simulations. The experimental $S(Q)$ are remarkably well reproduced by the MD simulation, although the height of the first sharp diffraction peak (FSDP) observed at $1.5 < Q < 2.7\,\text{Å}^{-1}$ is slightly overestimated in the simulations (especially for 10 GPa). The observed FSDP position (see Table S1 in the Supplemental Material [27]) shows a drastic and almost linear increase up to 31 GPa, and the FSDP profile becomes much more subtle beyond this point, which is in excellent agreement with the previous studies at least up to 100 GPa [7,8,12,17]. The second principal peak (PP) observed around $Q \sim 3\,\text{Å}^{-1}$, which has previously been considered as a manifestation of the presence of octahedrally (sixfold)-coordinated Si [12], becomes prominent above 31 GPa, and the peak position gradually shifts to a higher-Q region with increasing pressure up to 170 GPa. As shown in Fig. 2(b), this behavior is well understood in terms of partial structure factors, $S_{\alpha\beta}(Q)$, in which the evolution of the silicon-silicon principal peak increases with increasing pressure.

To understand the short-range structure in detail, the average Si-O bond length as a function of pressure was determined based on the first $T(r)$ peak position as well as the

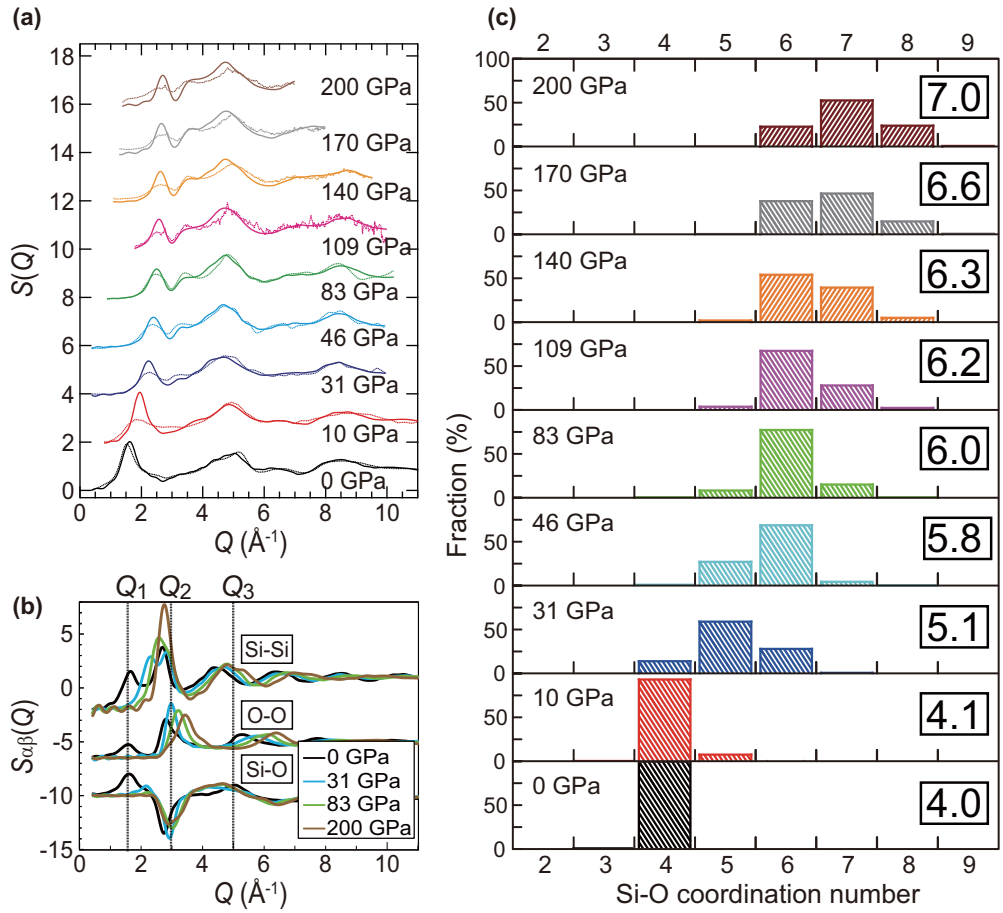

FIG. 2. High-pressure structural data and pressure evolution of Si-O coordination number of SiO_2 glass. (a) X-ray total structure factors $S(Q)$ of SiO_2 glass up to pressures of 200 GPa. Dotted curves: experimental data; solid curves: MD simulations. (b) Faber-Ziman partial structure factors of $S_{SiSi}(Q)$, $S_{SiO}(Q)$, and $S_{OO}(Q)$ up to 200 GPa. The approximate principal peak positions as labeled by Q_1, Q_2, and Q_3 observed under ambient condition are indicated by the vertical broken lines. (c) Distribution of the Si-O coordination number in SiO_2 glass as a function of pressure up to 200 GPa. The number in the square denotes the average Si-O coordination number at each pressure.

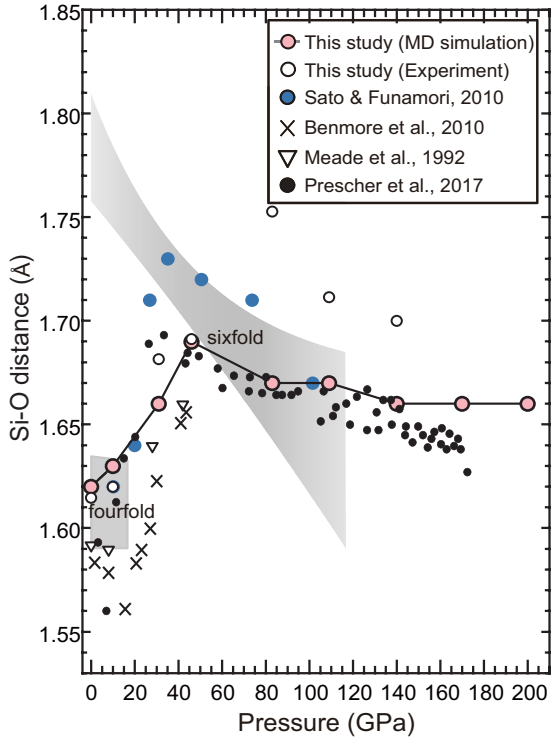

FIG. 3. Pressure dependence of the Si-O bond length of silica glass up to pressures of 140 GPa together with the previous results [8,12,17,21]. The shaded areas represent the range of Si-O bond lengths for crystalline silica phases with fourfold- and sixfold-coordinated [38] structures.

MD simulations in real space (Fig. S1 in the Supplemental Material [27]), and the numerical values are shown in Fig. 3 together with the previous results [8,12,17,21]. Although there are some differences due to pressure conditions and insufficient real-space resolution in the experimental data (especially above 83 GPa), the same trend of the Si-O bond lengths is observed among the experimental and MD simulations results. The results indicate that the average Si-O distance increases monotonically with pressure at least up to 46 GPa and turns to decline to 140 GPa, and eventually becomes constant up to 200 GPa. The overall trend of our results is consistent with those of Sato and Funamori [17] up to ~100 GPa and Prescher *et al.* up to 174 GPa [21]. According to the estimated bond lengths of the sixfold-coordinated crystalline SiO_2 phase [38] shown as the shaded area in Fig. 3, we suggest that the sixfold-coordinated silicon in SiO_2 glass becomes predominant at pressure approaching 40 GPa.

Intermediate-range ordering in AX_2 glasses is of particular interest because the typical examples of SiO_2 and GeO_2 are very well known as glass-forming materials according to Zachariasen's theory [39]. Therefore, it is indispensable to investigate the relationship between the intermediate-range/chemical ordering and the behavior of the FSDP/second PP in the structure factor. Although the MD simulations overestimate the FSDP heights, those observed for $S_{SiSi}(Q)$ and $S_{OO}(Q)$ appear to disappear at 31 GPa [Fig. 2(b)]. Another remarkable feature is the very sharp PP observed at $Q \sim 2.75$ Å in $S_{SiSi}(Q)$, which is also observed in x-ray diffraction data [see Fig. 2(a)]. The PP is usually observed at $Q \sim 3$ Å^{-1} in neutron diffraction data at ambient to low pressures because it reflects the packing of oxygen atoms [40,41]. However, our analyzed data suggest that the very intense PP in the x-ray diffraction data is a signature of increased packing fraction of silicon associated with the formation of tricluster and tetracluster configurations, while the PP in $S_{OO}(Q)$ do not change significantly [Fig. 2(b)]. These observations show a clear tendency for the pressure-induced deformation of intermediate-range topological ordering associated with chemical ordering manifested by the evolution of PP. Such a significant diminution of FSDPs with pressure is likely associated with the possible disturbance of the evolution of intermediate-range ordering caused by the pressure-induced diversification of coordination states and polyhedral linkages including an edge-shared connection observed in liquid ZrO_2 [42].

B. Si-O coordination numbers

The distributions of Si-O coordination numbers were derived from the MD models and are shown in Fig. 2(c) where the gradual changes from fourfold to higher coordination can be clearly observed. The fourfold-coordinated structure retains up to 10 GPa almost as a single coordination species. The fivefold-coordinated structure becomes predominant at 31 GPa. The dominant coordination state subsequently shifts to sixfold at the pressure regime between 46 and 109 GPa. Here, a significant rise in the proportion of sevenfold coordination is visible, whereas the fraction of fivefold-coordinated configuration decreases as a compensation. Such a coordination number change with pressure is in a good agreement with the previous results up to 109 GPa [8,12,17] and up to 174 GPa [21]. However, it is found that the fraction of the sevenfold-coordination state increases up to 40% at 140 GPa and becomes eventually greater than that of sixfold above 170 GPa, reaching a fraction of 53% at 200 GPa. The remarkable feature shown here is that the SiO_2 glass does not comprise a single coordination state under pressure but exhibits a broader distribution above 31 GPa, such as SiO_6 and SiO_7 polyhedra. Furthermore, the average coordination number is found to change gradually as the coordination distributions evolve. While the observed declining trend in the Si-O bond length at pressures approaching 140 GPa indicates a stable sixfold-coordination state which behaves as the crystalline form of silica, the trend above 170 GPa showing the constant value can be interpreted as the onset of the average coordination number higher than 6. The corresponding snapshot of the local environment around oxygen atoms at 200 GPa constructed based on the MD simulation [Fig. 4(a)] highlights the formation of tricluster (OSi_3) and/or tetracluster (OSi_4) configurations. Furthermore, Voronoi polyhedral analysis [43] also implies the formation of the SiO_6 and SiO_7 polyhedra. With a careful inspection of such polyhedral atomic configurations, we find that the Si-O polyhedra exhibit a large variety of distorted features which deviate from the ideal regular polyhedral structures, as shown in Fig. S2 in the Supplemental Material [27].

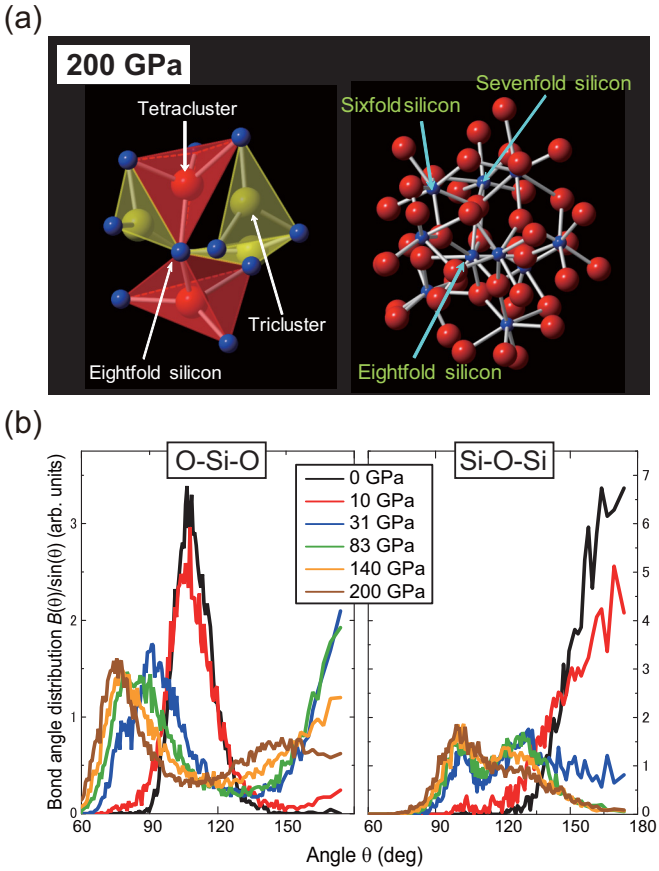

FIG. 4. Atomic structure and bond angle distribution of SiO_2 glass under high pressure. (a) Snapshot of the local environment around oxygen atoms at 200 GPa, highlighting the oxygen tricluster and tetracluster configurations (O coordinated with three or four silicon). Blue spheres: silicon atoms; yellow spheres: oxygen atoms. (b) Pressure dependence of the O-Si-O (left) and Si-O-Si (right) bond angle distribution up to 200 GPa.

C. Bond angle distribution and polyhedral connection

To uncover the atomic structure in SiO_2 glass at high pressures, we have calculated bond angle distributions with pressure, and they are shown as O-Si-O and Si-O-Si configurations in Fig. 4(b). The O-Si-O bond angle distribution at 0 GPa shows a fairly sharp maximum close to 109.4° as expected for a regular SiO_4 tetrahedron. The maximum peak position gradually gets smaller down to ∼90° up to 83 GPa, and the peak distribution becomes distorted with a broad shoulder at larger angles above ∼110°. Although the sixfold-coordinated structure is presumed to be the major component at 83 GPa, the corresponding angle distributions largely deviate from the ideal O-Si-O angle of 90° for a regular octahedron. The broad feature is consistent with the broad Si-O coordination number distribution at high pressure [Fig. 2(c)], suggesting that the changes in bond angle distributions are due to the wide variety of O coordination around Si at high pressures.

The features of O-Si-O bond angles at 200 GPa distinctively differ from those observed at lower pressures. The peaks around 75° and 145° are highly analogous to those observed in the random packing structure of hard spheres, indicating that the structure of SiO_2 glass under ultrahigh pressure is very different from that at ambient pressure. Taken into account our results for the short-range structure, the appearance of such peak/shoulders correlates with the formation of sevenfold or higher coordinated structures in a highly distorted polyhedral geometry, which is in line with the results of Voronoi analysis.

The Si-O-Si bond angle distribution shows a peak towards 180° up to 10 GPa, which is a signature of a tetrahedral network. On the other hand, the position of the peak shifts to a small-angle region from 31 GPa and shows two peaks around 103° (OSi_4 tetracluster) and 124° (OSi_3 tricluster) at 140 GPa. The latter peak is not obvious at 200 GPa, suggesting that OSi_4 tetracluster becomes more dominant.

In order to shed further light on the nature of the atomic arrangement, the total volume of cavities ("voids") and polyhedral connections for SiO_n polyhedra were calculated and are summarized in Table S2 in the Supplemental Material [27]. The fraction of cavity volumes exhibits a drastic decrease with pressure and there are essentially no cavities above 31 GPa, while the SiO_2 glass initially has a cavity volume of 36.8% at ambient pressure. Previously, it has been considered that the presence of interstitial cavities in the SiO_2 glasses/melts indicates a potential ability to store noble gases, such as helium and argon, within the disordered structures [44]. The rapid decrease in the cavity volume with pressure approaching 30 GPa offers a feasible explanation for the observation in the previous high-pressure experiments where the solubility of noble gases in SiO_2 melts/glasses drastically decreased at pressures around 10–20 GPa [44].

Table S2 and Fig. S3 in the Supplemental Material [27] also show the pressure-induced change in the polyhedral connections for SiO_n. The connections initially display 100% of corner-shared configurations at ambient pressure, and they show a gradual transition from corner-shared to edge-shared structures together with a minor fraction of face-shared structures.

D. Topological nature

To elucidate the structural information that cannot be sufficiently analyzed by the conventional methods from atomic configurations, we applied a topological/mathematical method using persistent homology for characterizing the geometrical features in amorphous materials [22]. This method is primarily based on the persistence diagram (PD) which can visualize the persistent homology two dimensionally, and thus various topological features such as ring structures and polyhedral connections/distortions can be monitored.

Figures 5(a)–5(g) show Si-centric PDs $D(\mathrm{Si})_1$, which describe the geometrical features of silicon atoms for the topological dimensionality of 1. We compare 0, 31, 83, and 200 GPa data together with stishovite ($d = 4.28\,\mathrm{g/cm^3}$) [45], α-PbO_2 type ($d = 4.30\,\mathrm{g/cm^3}$) [46], and pyrite type ($d = 6.58\,\mathrm{g/cm^3}$) [47]. With those PDs, we can extract the geometrical information of the atoms primarily associated with the one-dimensional linkages such as rings. The profiles along with the death line highlighted by colors are shown in Fig. 5(h). In the case of the crystalline phase, we can observe a systematic peak shift to small death value with increasing density. It is found that a vertical and broad profile along with

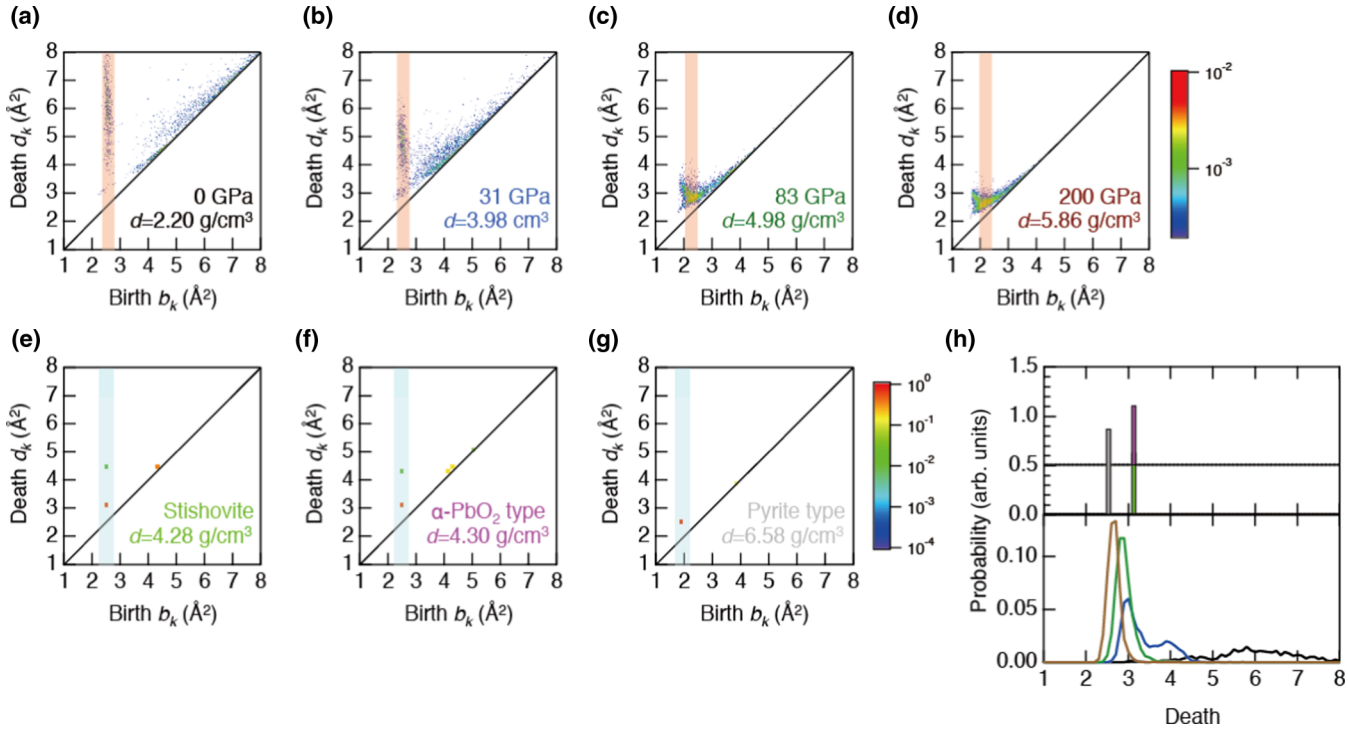

FIG. 5. Analysis using Si-centric persistent homology for the topological dimensionality of 1. (a)–(g) Si-centric persistence diagrams $D(\mathrm{Si})_1$ at 0, 31, 83, and 200 GPa. (h) The probability profiles along with the death line highlighted by colors. Black line: 0 GPa; blue line: 31 GPa; green line: 83 GPa; and brown line: 200 GPa. Light green: stishovite; pink: α-PbO_2-type SiO_2; gray: pyrite-type SiO_2.

the death line observed at birth $= 2.6\,\text{Å}^2$ at ambient pressure in glass almost disappears at 31 GPa and an intense profile in both vertical and horizontal appears near the diagonal line at birth $\sim 3\,\text{Å}^2$. This behavior is a good descriptor for FSDP and is consistent with the observation of tricluster and tetracluster configurations under high pressures. Furthermore, the peak of glass at 200 GPa is very close to pyrite-type data, although the density of the glass is much smaller than the crystalline phase. Similar behavior is observed in O-centric PDs $D(\mathrm{O})_1$ shown in Fig. S4 in the Supplemental Material [27].

Figures S5(a)–S5(g) in the Supplemental Material [27] shows Si-centric PDs $D(\mathrm{Si})_2$ of glasses and three crystalline phases, which describe the geometrical features of the silicon atoms for the topological dimensionality of 2. With those PDs, we can extract the geometrical information of the atoms primarily associated with the two-dimensional connections such as polyhedral formation with the reduction of cavity volume. The geometrical configurations having all those characteristics observed above 31 GPa no longer represent a network structure, but rather a dense-packed structure [22]. The profiles along with the diagonal line highlighted by colors are shown in Fig. S5(h) in the Supplemental Material [27]. The birth value of the broad prole along with the diagonal line rapidly decreases and multiplicity is increased with increasing pressure, which is in line with the behavior of $D(\mathrm{Si})_1$ (Fig. 5). In addition, the profile of glass at 200 GPa is similar to that of the pyrite-type crystalline phase. On the other hand, O-centric PDs $D(\mathrm{O})_2$ [Figs. 6(a)–6(g)] show that some data initially distributed along the diagonal line at lower pressure get gradually deviated in a direction toward the upper left from the diagonal line with pressure and, eventually, appear to form the isolated clusterlike "island" at 200 GPa apart from the original distribution. The profiles along with the death line highlighted by colors are shown in Fig. 6(h), which shows similar behavior with silicon atoms. With the analyses of persistent homology, the emergence of such "islandlike" deviation is found to correspond to the formation of the octahedrally coordinated oxygen atoms (that is SiO_6), whereas the distribution along the diagonal indicates the presence of the oxygen tetrahedra (SiO_4). This interpretation is remarkably compatible with our earlier findings. In addition, recent topological analyses for the metallic glass with highly dense-packed structure [21] also showed the very similar topological nature in PDs to that obtained under the higher-pressure condition in this study, again indicating that the densification is achieved by the gradual transition from network structure to dense-packed structure in conjunction with a change in the coordination state.

As can be seen in Fig. 2(b), $S_{\mathrm{SiSi}}(Q)$ is very sensitive to pressures above 31 GPa, while that of the PP in $S_{\mathrm{OO}}(Q)$ is highly insensitive, which is highly correlated with the pressure-induced changes in PDs D_1 and D_2, respectively. These behaviors are also very far away from those in densification at lower pressure reported by Zeidler *et al.* [40]. Pressure-induced structural change in our study could therefore be categorized into the pressure-induced "topological disorder" in the intermediate length scale associated with chemical ordering under ultrahigh pressure [48]. This implies that only high pressure can produce such an unusual glass structure at room temperature. Furthermore, our finding paves the way for the synthesis of different families of highly disordered, dense glasses from various oxides (including

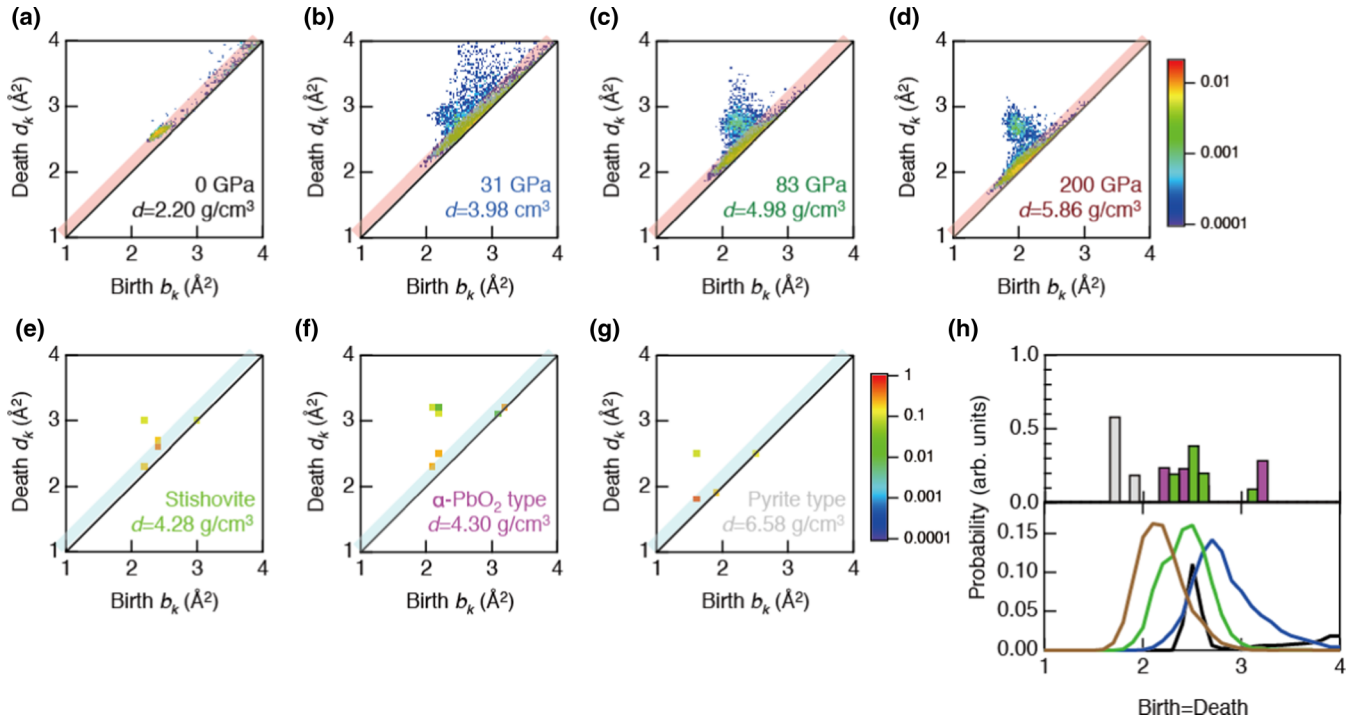

FIG. 6. Analysis using O-centric persistent homology for the topological dimensionality of 2. (a)–(g) O-centric persistence diagrams for $D(O)_2$ at 0, 31, 83, and 200 GPa. (h) The probability profiles along with the diagonal line highlighted by colors. Black line: 0 GPa; blue line: 31 GPa; green line: 83 GPa; and brown line: 200 GPa. Light green: stishovite; pink: α-PbO_2-type SiO_2; gray: pyrite-type SiO_2.

cases with low glass-forming ability) by applying ultrahigh pressure.

Recently, Zeidler *et al.* [40] proposed a groundbreaking concept on the relationship between coordination numbers and oxygen packing fractions (OPF) in oxide glasses, which gives a universal picture of the coordination number evolution under pressure. This concept is highly supported by the recent high-pressure experimental results on GeO_2 glass up to 100 GPa [49], strengthening the predictability of this concept towards configurations under extreme pressures. According to the extrapolated calculations with some assumptions for OPF in SiO_2 glass from previous calculations [8,16,17], the onset pressure where the Si-O coordination number becomes higher than 6 is expected around 108 GPa [49]. This is consistent with the present results for OPFs up to 200 GPa shown in Fig. S6 of the Supplemental Material [27], and supports our previous results for sound velocity as well [18].

E. DFT simulations

We have shown above that the SiO_2 glass undergoes a transition from network- to dense-packed structure in conjunction with the coordination number change under high pressure. It is expected that most substances that are dense packed ultimately become metallic under extreme pressures, and the question arises whether the SiO_2 glass expresses metallic features under ultrahigh-pressure conditions approaching 200 GPa. To address this issue and to reveal the effects of the changes in Si-O coordination number on electronic states, we computed the electronic structures of the SiO_2 glass by DFT calculations based on the structural models discussed above (samples of 3000 atoms, fixed volume). The DFT results for the effective charges (Q_{eff}) and atomic volumes (V_{at}) of Si and O atoms are listed in Table S3 in the Supplemental Material [27]. The effective charges are remarkably insensitive to pressure exhibiting values close to $+2$ for Si and -1 for O. On the other hand, the atomic volume of Si appears to decrease monotonically with pressure, whereas the same for O shows a drastic reduction of as much as 50% within the pressure range 0–31 GPa. Since the atomic volume is mainly assigned to O within the Voronoi script, this significant reduction of atomic volumes of O with no changes in the electronic structure and effective charges corresponds to the disappearance of cavity volumes between 0 and 31 GPa (Table S2 in the Supplemental Material [27]) as described above. The reduced volume of O together with the disappearing cavities stimulates the formation of SiO_6 from SiO_4, which is also observed to have its onset around 30 GPa. Owing to such rapid changes in V_{at}, the O and Si volumes approach each other at higher pressures, supporting, again, the conclusion that SiO_2 glass undergoes structural changes in line with the hard-sphere-like dense packing without any metallic signature.

The electronic structure of SiO_2 glass under pressure was analyzed based on the electronic density of states (DOS). Figure 7 shows the DOS of SiO_2 glass with projections onto different elements, P-DOS. The distribution of the P-DOS bands is found to become broader with increasing pressure, which reflects the wider distribution of the oxygen coordination number around silicon under high pressures. Despite these changes, the band gaps at the Fermi energy become wider with pressure, as shown in Fig. 7, implying that the system remains insulating under pressure. The structural diversity

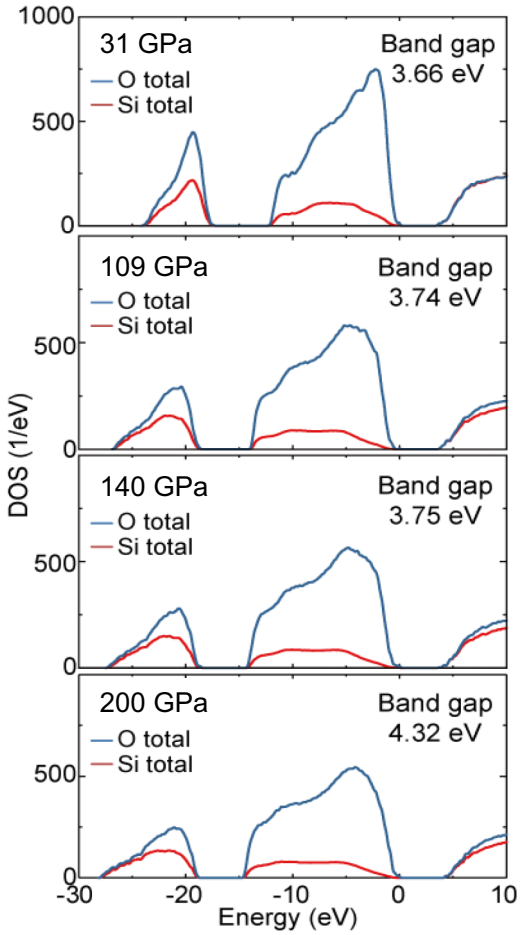

FIG. 7. Electronic structure of silica glass under high pressure. The electronic density of states (DOS) of the SiO_2 glass with projections onto O and Si up to 200 GPa.

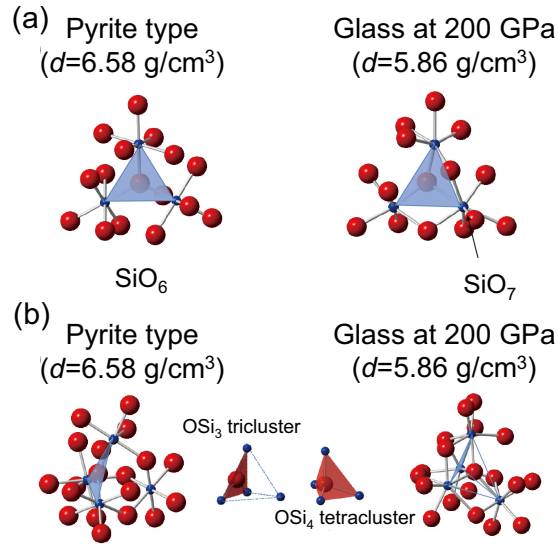

FIG. 8. Local structures of pyrite-type crystalline SiO_2 and SiO_2 glass (at 200 GPa) extracted from persistence diagram. (a) SiO_x polyhedra extracted from Si-centric persistent homology for the topological dimensionality of 1. (b) OSi_y clusters extracted from Si-centric persistent homology for the topological dimensionality of 2.

has normally been considered to make the band gap narrower [42], which seems contradictory to the fact that our results show apparent structural varieties with pressure. One possible reason may be the increase in bond angle symmetry for Si-O-Si, whereas the symmetry of O-Si-O decreases with pressure, as can be seen in Fig. 4(b). If this is the case, the formation of overcoordinated oxygen with relatively symmetric bond angles may secure the insulation property of the SiO_2 glass under high pressure.

To manifest the topology in silica glass under ultrahigh pressures, we extract the atomic configurations which give an intense multiplicity for $D(\mathrm{Si})_1$ and $D(\mathrm{Si})_2$ of pyrite-type crystal and glass at 200 GPa and shown in Figs. 8(a) and 8(b), respectively. Intriguingly, PD analyses can provide us with information about triclusters and tetraclusters from $D(\mathrm{Si})_1$ and $D(\mathrm{Si})_2$, respectively. Pyrite-type crystal is comprised of only SiO_6 octahedra (OSi_3 tricluster). On the other hand, the formation of a SiO_7 polyhedron is observed in glass as well as SiO_6 octahedra, but its topology is very similar to pyrite-type crystal [see Fig. 8(a)]. As can be seen in Fig. 8(b), tricluster in pyrite-type crystal can be extracted from PD analysis (see left panel), while the formation of OSi_4 tetracluster is observed in glass at 200 GPa (right panel). However, it is found that the tetracluster is highly distorted (oxygen atom is off center) and the topology is very similar to $OSi_3 + Si$, in pyrite-type crystal. We suggest that the topological similarity between glass at 200 GPa and pyrite-type crystal would be caused by the distortion of oxygen clusters and the variety of Si-O coordination in terms of disorder in glass.

IV. CONCLUSIONS

In this paper, we have investigated the topology of SiO_2 glass MD simulations supported by using the high-energy synchrotron x-ray diffraction technique and topological analyses in a pressure range up to 200 GPa. Our results reveal that the SiO_2 glass undergoes a coordination number change from six to seven at pressure approaching 200 GPa. The atomistic modeling demonstrates the formation of unusual densely arranged local structures around O atoms, such as tricluster (OSi_3) or tetracluster (OSi_4) configurations. The topological analyses succeed in visually discriminating the Si-O coordination changes between fourfold and sixfold using PDs, and reveal that the high-pressure form of the SiO_2 glass exhibits highly distorted structural features, which have so far been unable to be seen by the use of incoherent x-rays and conventional analysis tools with defining coordination distances (pair-correlation function, bond angle distribution, and so on). Furthermore, we observed the topological similarity between glass and crystal with higher density under ultrahigh pressure. This also strongly offers a direction in future experiments to determine hidden local symmetries in pair correlation by cross-correlation analysis employing coherent x-rays [50]. The results also demonstrate that the coordination number change of SiO_2 glass no longer follows that of the crystalline SiO_2 phase under ultrahigh pressures since the sixfold-coordinated structure is believed to persist, at least, up to ~700 GPa for the latter case [51]. The evolution

of Si-O coordination number appears to remarkably follow the universal path for OPF with pressure, as proposed by Zeidler *et al.* [40]. This pronounced difference between the glass and crystalline phase in pressure-induced structural change is most likely caused by the potential structural tolerance in the glass for accepting the distortion to a certain extent, which might allow the glasses to have unusually higher coordination numbers that cannot be achieved in the crystalline phase at an equivalent condition.

ACKNOWLEDGMENTS

The synchrotron radiation experiments were performed under the approval of the Japan Synchrotron Radiation Research Institute (JASRI) (Proposals No. 2009A1064, No. 2010A1048, No. 2010B1092, No. 2011A1239, No. 2011B1159, No. 2011B1153, No. 2013B1217). This research was supported by JSPS KAKENHI Grant Nos. JP22684028, JP24654170, JP25247087, JP15KK0148, a Grant for Program Research from Frontier Research Institute for Interdisciplinary Sciences, Tohoku University, and the Start-up funds at ETH Zürich (M.M.). This work was supported by JST PRESTO Grant No. JPMPR15N4, Japan (S.K.) and "Materials research by Information Integration" Initiative (MI2I) project of the Support Program for Starting Up Innovation Hub from JST (S.K., Y.H.) and JST CREST Grant No. 15656429 (Y.H.). The DFT calculations were carried out on the Cray XT4/XT5 computers at CSC, IT Center for Science Ltd., Finland, and Cray XC30 in Japan Advanced Institute of Science and Technology, Japan. J.A., J.K., T.M., and A.S.F. acknowledge financial support from the Academy of Finland through its Centres of Excellence Program (Project No. 284621).

M.M. and S.K. designed the research conception. M.M. and N.H. conducted *in situ* high-pressure synchrotron x-ray diffraction experiments. S.K. performed the atomic structural analyses. H.I. constructed the structural model using MD simulations. N.K. and J.A. contributed to the electronic structural analyses. A.H., Y.H., and I.O. were involved in the topological analyses. T.M., A.S.F., and J.A. tested various parameterizations of the interatomic potentials for MD simulation. N.H. and Y.O. contributed to the optimization of *in situ* synchrotron x-ray diffraction measurements. Y.O. calculated the OPFs. J.K. and J.A. contributed to the cavity analyses. O.S. and Y.I. were involved in the data analyses for atomic and electronic structures, respectively.

The authors declare no conflict of interest.

[1] F. S. El'kin, V. V. Brazhkin, L. G. Khvostantsev, O. Tsiok, and A. G. Lyapin, *In situ* study of the mechanism of formation of pressure-densified SiO_2 glasses, J. Exp. Theor. Phys. Lett. **75**, 342 (2002).

[2] P. W. Bridgman, The compressibility of several artificial and natural glasses, Am. J. Sci. **10**, 359 (1925).

[3] P. W. Bridgman, The effect of pressure on the tensile properties of several metals and other materials, J. Appl. Phys. **24**, 560 (1953).

[4] K. Trachenko and M. T. Dove, Compressibility, kinetics, and phase transition in pressurized amorphous silica, Phys. Rev. B **67**, 064107 (2003).

[5] J. F. Shackelford and J. S. Masaryk, The interstitial structure of vitreous silica, J. Non. Cryst. Solids **30**, 127 (1978).

[6] D. J. Lacks, First-Order Amorphous-Amorphous Transformation in Silica, Phys. Rev. Lett. **84**, 4629 (2000).

[7] T. Sato and N. Funamori, Sixfold-Coordinated Amorphous Polymorph of SiO_2 Under High Pressure, Phys. Rev. Lett. **101**, 255502 (2008).

[8] C. J. Benmore, E. Soignard, S. A. Amin, M. Guthrie, S. D. Shastri, P. L. Lee, and J. L. Yarger, Structural and topological changes in silica glass at pressure, Phys. Rev. B **81**, 054105 (2010).

[9] R. J. Hemley, H. K. Mao, P. M. Bell, and B. O. Mysen, Raman-Spectroscopy of SiO_2 Glass at High-Pressure, Phys. Rev. Lett. **57**, 747 (1986).

[10] Q. Williams and R. Jeanloz, Spectroscopic evidence for pressure-induced coordination changes in silicate-glasses and melts, Science **239**, 902 (1988).

[11] Y. Inamura, Y. Katayama, W. Utsumi, and K.-i. Funakoshi, Transformations in the Intermediate-Range Structure of SiO_2 Glass under High Pressure and Temperature, Phys. Rev. Lett. **93**, 015501 (2004).

[12] C. Meade, R. J. Hemley, and H. Mao, High-Pressure X-ray Diffraction of SiO_2 Glass, Phys. Rev. Lett. **69**, 1387 (1992).

[13] M. Grimsditch, Polymorphism in Amorphous SiO_2, Phys. Rev. Lett. **52**, 2379 (1984).

[14] C.-s. Zha, R. J. Hemley, H.-k. Mao, T. S. Duffy, and C. Meade, Acoustic velocities and refractive index of SiO_2 glass to 57.5 GPa by Brillouin scattering, Phys. Rev. B **50**, 13105 (1994).

[15] J.-F. Lin, H. Fukui, D. Prendergast, T. Okuchi, Y. Q. Cai, N. Hiraoka, C.-S. Yoo, A. Trave, P. Eng, M. Y. Hu, and P. Chow, Electronic bonding transition in compressed SiO_2 glass, Phys. Rev. B **75**, 012201 (2007).

[16] A. Zeidler, K. Wezka, R. F. Rowlands, D. A. J. Whittaker, P. S. Salmon, A. Polidori, J. W. E. Drewitt, S. Klotz, H. E. Fischer, M. C. W. Craig, M.-G. Tucher and M. Wilson, High-Pressure Transformation of SiO_2 Glass from a Tetrahedral to an Octahedral Network: A Joint Approach Using Neutron Diffraction and Molecular Dynamics, Phys. Rev. Lett. **113**, 135501 (2014).

[17] T. Sato and N. Funamori, High-pressure structural transformation of SiO_2 glass up to 100 GPa, Phys. Rev. B **82**, 184102 (2010).

[18] M. Murakami and J. D. Bass, Spectroscopic Evidence for Ultrahigh-Pressure Polymorphism in SiO_2 Glass, Phys. Rev. Lett. **104**, 025504 (2010).

[19] V. Brazhkin, A. Lyapin, and K. Trachenko, Atomistic modeling of multiple amorphous-amorphous transitions in SiO_2 and GeO_2 glasses at megabar pressures, Phys. Rev. B **83**, 132103 (2011).

[20] M. Wu, Y. Liang, J.-Z. Jiang, and S. T. John, Structure and properties of dense silica glass, Sci. Rep. **2**, 398 (2012).

[21] C. Prescher, V. B. Prakapenka, J. Stefanski, S. Jahn, L. B. Skinner, and Y. Wang, Beyond sixfold coordinated Si in SiO_2 glass at ultrahigh pressures, Proc. Natl. Acad. Sci. USA **114**, 10041 (2017).

[22] Y. Hiraoka, T. Nakamura, A. Hirata, E. G. Escolar, K. Matue, and Y. Nishiura, Hierarchical structures of amorphous solids characterized by persistent homology, Proc. Natl. Acad. Sci. USA **113**, 7035 (2016).

[23] Y. Ohishi, N. Hirao, N. Sata, K. Hirose, and M. Takata, Highly intense monochromatic X-ray diffraction facility for high-pressure research at SPring-8, High Press. Res. **28**, 163 (2008).

[24] Y. Akahama and H. Kawamura, High-pressure Raman spectroscopy of diamond anvils to 250 GPa: Method for pressure determination in the multimegabar pressure range, J. Appl. Phys. **96**, 3748 (2004).

[25] H. Mao, J.-A. Xu, and P. Bell, Calibration of the ruby pressure gauge to 800 kbar under quasi-hydrostatic conditions, J. Geophys. Res. **91**, 4673 (1986).

[26] S. Kohara *et al.*, Z. Phys. Chem. **230**, 339 (2016).

[27] See Supplemental Material at http://link.aps.org/supplemental/10.1103/PhysRevB.99.045153 for more information regarding the atomic, electronic, and topological nature of the SiO_2 glass under high pressure condition. The Supplemental Material contains Refs. [8,16,17,52–56].

[28] A. C. Van Duin, S. Dasgupta, F. Lorant, and W. A. Goddard, ReaxFF: A reactive force field for hydrocarbons, J. Phys. Chem. **105**, 9396 (2001).

[29] T.-R. Shan, D. Bryce, J. Hawkins, A. Asthagiri, S. Phillpot, and S. Sinnott, Second-generation charge-optimized many-body potential for Si/SiO_2 and amorphous silica, Phys. Rev. B **82**, 235302 (2010).

[30] J. Horbach, Molecular dynamics computer simulation of amorphous silica under high pressure, J. Phys.: Condens. Matter **20**, 244118 (2008).

[31] B. W. H. van Beest, G. J. Kramer, and R. A. van Santen, Force Fields for Silicas and Aluminophosphates Based on *Ab Initio* Calculations, Phys. Rev. Lett. **64**, 1955 (1990).

[32] J. Akola and R. Jones, Structural phase transitions on the nanoscale: The crucial pattern in the phase-change materials $Ge_2Sb_2Te_5$ and GeTe, Phys. Rev. B **76**, 235201 (2007).

[33] J. VandeVondele, M. Krack, F. Mohamed, M. Parrinello, T. Chassaing, and J. Hutter, Quickstep: Fast and accurate density functional calculations using a mixed Gaussian and plane waves approach, Comput. Phys. Commun. **167**, 103 (2005).

[34] J. Hutter, M. Iannuzzi, F. Schiffmann, and J. VandeVondele, CP2K: Atomistic simulations of condensed matter systems, Wiley Interdiscip. Rev.: Comput. Mol. Sci. **4**, 15 (2014).

[35] J. VandeVondele and J. Hutter, Gaussian basis sets for accurate calculations on molecular systems in gas and condensed phases, J. Chem. Phys. **127**, 114105 (2007).

[36] S. Goedecker, M. Teter, and J. Hutter, Separable dual-space Gaussian pseudopotentials, Phys. Rev. B **54**, 1703 (1996).

[37] J. P. Perdew, K. Burke, and M. Ernzerhof, Generalized Gradient Approximation Made Simple, Phys. Rev. Lett. **77**, 3865 (1996).

[38] D. Andrault, G. Fiquet, F. Guyot, and M. Hanfland, Pressure-induced Landau-type transition in stishovite, Science **282**, 720 (1998).

[39] W. H. Zachariasen, The atomic arrangement in glass, J. Am. Chem. Soc. **54**, 3841 (1932).

[40] A. Zeidler, P. S. Salmon, and L. B. Skinner, Packing and the structural transformations in liquid and amorphous oxides from ambient to extreme conditions, Proc. Natl. Acad. Sci. USA **111**, 10045 (2014).

[41] A. Zeidler and P. S. Salmon, Pressure-driven transformation of the ordering in amorphous network-forming materials, Phys. Rev. B **93**, 214204 (2016).

[42] S. Kohara, J. Akola, L. Patrikeev, M. Ropo, K. Ohara, M. Itou, A. Fujiwara, J. Yahiro, J. T. Okada, T. Ishikawa, A. Mizuno, A. Masuno, Y. Watanabe, and T. Usuki, Atomic and electronic structures of an extremely fragile liquid, Nat. Commun. **5**, 5892 (2014).

[43] T. Fukunaga, K. Itoh, T. Otomo, K. Mori, M. Sugiyama, H. Kato, M. Hasegawa, A. Hirata, Y. Hirotsu, and A. C. Hannon, Voronoi analysis of the structure of Cu–Zr and Ni–Zr metallic glasses, Intermetallics **14**, 893 (2006).

[44] A. Paonita, Noble gas solubility in silicate melts: A review of experimentation and theory, and implications regarding magma degassing processes, Ann. Geophys. **48**, 647 (2005).

[45] N. L. Ross, J. Shu, and R. M. Hazen, High-pressure crystal chemistry of stishovite, Am. Mineral. **75**, 739 (1990).

[46] P. Dera, C. T. Prewitt, N. Z. Boctor, and R. J. Hemley, Characterization of a high-pressure phase of silica from the Martian meteorite Shergotty, Am. Mineral. **87**, 1018 (2002).

[47] Y. Kuwayama, K. Hirose, N. Sata, and Y. Ohishi, The pyrite-type high-pressure form of silica, Science **309**, 923 (2005).

[48] P. S. Salmon, A. C. Barnes, R. A. Martin, and G. J. Cuello, Glass Fragility and Atomic Ordering on the Intermediate and Extended Range, Phys. Rev. Lett. **96**, 235502 (2006).

[49] Y. Kono, C. Kenney-Benson, D. Ikuta, Y. Shibazaki, Y. Wang, and G. Shen, Ultrahigh-pressure polyamorphism in GeO_2 glass with coordination number >6, Proc. Natl. Acad. Sci. USA **113**, 3436 (2016).

[50] P. Wochner, C. Gutt, T. Autenrieth, T. Demmer, V. Bugaev, A. D. Ortiz, A. Duri, F. Zontone, G. Grubel, and H. Dosch, X-ray cross correlation analysis uncovers hidden local symmetries in disordered matter, Proc. Natl. Acad. Sci. USA **106**, 11511 (2009).

[51] S. Wu, K. Umemoto, M. Ji, C.-Z. Wang, K.-M. Ho, and R. M. Wentzcovitch, Identification of post-pyrite phase transitions in SiO_2 by a genetic algorithm, Phys. Rev. B **83**, 184102 (2011).

[52] K. Wezka, P. S. Salmon, A. Zeidler, D. A. Whittaker, W. E. Drewitt, S. Klotz, H. E. Fischer, and D. Marrocchelli, Mechanisms of network collapse in GeO_2 glass: High-pressure neutron diffraction with isotope substitution as arbitrator of competing models, J. Phys.: Condens. Matter **24**, 502101 (2012).

[53] J. W. Drewitt, P. S. Salmon, A. C. Barnes, S. Klotz, H. E. Fischer, and W. A. Crichton, Structure of GeO_2 glass at pressures up to 8.6 GPa, Phys. Rev. B **81**, 014202 (2010).

[54] P. S. Salmon, J. W. E. Drewitt, D. A. J. Whittaker, A. Zeidler, K. Wezka, C. L. Bull, M.-G. Tucher, M. C. Cilding, M. Guthrie, and D. Marrocchelli, Density-driven structural transformations in network forming glasses: A high-pressure neutron diffraction study of GeO_2 glass up to 17.5 GPa, J. Phys.: Condens. Matter **24**, 415102 (2012).

[55] M. Guthrie, C. A. Tulk, C. J. Benmore, J. Xu, J. L. Yarger, D. D. Klug, J. S. Tse, H.-k. Mao, and R. J. Hemley, Formation and Structure of a Dense Octahedral Glass, Phys. Rev. Lett. **93**, 115502 (2004).

[56] Q. Mei, S. Sinogeikin, G. Shen, S. Amin, C. J. Benmore, and K. Ding, High-pressure x-ray diffraction measurements on vitreous GeO_2 under hydrostatic conditions, Phys. Rev. B **81**, 174113 (2010).